Geochemistry, Geophysics, Geosystems®

RESEARCH ARTICLE
10.1029/2025GC012627

The Importance of Sample-to-Sensor Distance in Quantitative Micro(Paleo-)Magnetic Analysis

Rosa A. de Boer[1], Frenk Out[1], Bertwin M. de Groot[1], Martha E. Kosters[1], and Lennart V. de Groot[1]

[1]Paleomagnetic laboratory Fort Hoofddijk, Department of Earth Sciences, Utrecht University, Utrecht, The Netherlands

Key Points:

- We developed an automated system (JAMES) to enable sample placement with ±1 μm precision in a Quantum Diamond Microscope (QDM)
- A known sample-to-sensor distance is valuable for determining quantitative paleomagnetic information from magnetic microscopy
- Magnetic moments of individual grains and summed intensities of multiple grains are particularly sensitive to accurate sample-to-sensor distance

Correspondence to:

R. A. de Boer,
r.a.deboer1@uu.nl

Citation:

de Boer, R. A., Out, F., de Groot, B. M., Kosters, M. E., & de Groot, L. V. (2026). The importance of sample-to-sensor distance in quantitative micro(paleo-) magnetic analysis. *Geochemistry, Geophysics, Geosystems*, *27*, e2025GC012627. https://doi.org/10.1029/2025GC012627

Received 4 NOV 2025
Accepted 12 MAY 2026

Author Contributions:

Data curation: Rosa A. de Boer
Formal analysis: Rosa A. de Boer
Funding acquisition: Lennart V. de Groot
Investigation: Rosa A. de Boer
Methodology: Frenk Out, Bertwin M. de Groot, Martha E. Kosters
Supervision: Lennart V. de Groot
Visualization: Rosa A. de Boer
Writing – original draft: Rosa A. de Boer
Writing – review & editing: Frenk Out, Bertwin M. de Groot, Martha E. Kosters, Lennart V. de Groot

© 2026 The Author(s). Geochemistry, Geophysics, Geosystems published by Wiley Periodicals LLC on behalf of American Geophysical Union.
This is an open access article under the terms of the Creative Commons Attribution-NonCommercial License, which permits use, distribution and reproduction in any medium, provided the original work is properly cited and is not used for commercial purposes.

Abstract Information on the past of Earth's magnetic field can be retrieved from magnetic grains in rock samples. Micromagnetic Tomography (MMT) is a recently developed method that uses magnetic surface scans from a Quantum Diamond Microscope (QDM) combined with the position of magnetic grains in rock samples to calculate the magnetic moments of those grains. An important parameter for these calculations is the sample-to-sensor distance during the magnetic measurements. Until recently, sample placement in the QDM was typically done manually. To improve sample placement, we developed an automated sample placement system (JAMES). JAMES eases the sample placement process by enabling the positioning of the sample in the x and y direction, as well as positioning of the sample plan-parallel against the sensor or at a known distance from the sensor with a precision of ±1 μm. We evaluated the importance of a known sample-to-sensor distance for retrieving quantitative magnetic information with MMT. With a known distance, individual grain magnetic moments and summed intensities (summed magnetic moments of individual grains) can be accurately determined. The sample-to-sensor distance is less important for determining directions, when studying isolated grains with dipolar magnetic surface expressions. However, when grains do not meet those conditions, a known sample-to-sensor distance is required to determine accurate directions. JAMES is now a standard element in the MMT procedure, ensuring reliable and repeatable magnetic measurements with the QDM. This greatly improves the precision of the magnetic moment calculations in MMT and advances the extraction of magnetic information from rock samples.

Plain Language Summary Magnetic grains in rocks hold information on the history of Earth's magnetic field. Magnetic microscopy enables the analysis of the signals stored in these grains to reconstruct the past direction and strength of the field. To do this accurately, it is important to know the exact distance between the rock sample and the sensor of the magnetic microscope. We have developed a system that places samples with high precision, positioning them at a known and controlled distance from the sensor in the microscope. In this study, we show that this precise positioning is valuable for calculating the strength of the magnetic signals and for analyzing individual grains. This helps extract more information about the Earth's magnetic field history from rocks.

1. Introduction

Emerging techniques in magnetic microscopy are transforming the field of paleomagnetism and rock-magnetism. These techniques enable analysis of the magnetic signals of individual magnetic minerals in rock samples, providing insights that go beyond those obtained from traditional bulk rock measurements. Magnetic microscopy enables high-resolution imaging of magnetic fields in geological samples with unprecedented precision and accuracy. These techniques are often used for qualitative analyses, to study the magnetic sources in a rock and their mineralogy and remanent magnetization (e.g., Brenner et al., 2022; Fu et al., 2014; Hess et al., 2024). However, they can also be applied for quantitative determinations of the magnetic moments of individual magnetic carriers, representing the direction and intensity of the ancient magnetic field (e.g., Fu et al., 2021; Grappone et al., 2025; Qi et al., 2025; Steele et al., 2023). Quantitative magnetic microscopy interpretations enable the potential retrieval of paleodirections and paleointensities from samples that could previously not be interpreted. To apply these techniques for quantitative analysis, a mathematical inversion is inherently required to transform 2D data to 3D information, but this process results in a non-unique solution (Kellogg, 1929).

Micromagnetic Tomography (De Groot et al., 2018, 2021) is a recently developed technique used for studying the magnetic information stored in geological samples that solves the uniqueness problem. It involves a combination

of magnetic microscopy with a Quantum Diamond Microscope (Glenn et al., 2017; Levine et al., 2019; Scholten et al., 2021) and 3D imaging of magnetic carriers by micro-/nanoCT scanning. These data sets are combined and inverted to retrieve the magnetic moments of individual iron-oxide grains in rock samples. The individual magnetic moments can be analyzed separately, allowing for the selection and interpretation of only the reliable magnetic recorders in a sample. By removing the contribution of poorly behaving magnetic recorders, the quality of the magnetic interpretations is greatly improved. Since the calculated magnetic moment per grain depends on the cubed distance, a precisely known sample-to-sensor distance is vital. The influence and importance of this distance is the focus point of this study.

In the Quantum Diamond Microscope (QDM) a diamond sensor is positioned above a polished, flat surface of a rock sample to enable optimal interaction between the sensor and the magnetic field of the sample. Positioning the sample against the diamond sensor of the QDM is typically done manually, which gives the user limited control over the precise placement in x, y, and z space as maneuvering the sample can be quite challenging and time-consuming. Automating control over the sample-to-sensor distance is valuable for the measurement precision and accuracy of the QDM and will promote routine use of the QDM. Therefore, we developed an automated sample placement system (James Automates Manipulation of Earth Samples; JAMES). JAMES allows for precise and controlled placement of the sample against the sensor or at a known distance from the sensor, with precise control in the x and y direction. We used JAMES to evaluate the importance of the sample-to-sensor distance for Micromagnetic Tomography (MMT) in a series of standoff distance experiments. We carried out bulk inversions and individual grain inversions on our experimental results, to determine the effect of the sample-to-sensor distance on the retrieval of magnetic moments.

The interpretation of QDM data and other magnetic surface maps is often done by means of upward continuation, where the magnetic moment is calculated by extrapolating magnetic data to larger distances from the sample (Blakely, 1996; Fu et al., 2020; Lima et al., 2014; Lima & Weiss, 2009, 2016; Oda et al., 2024). However, this averages the magnetic contributions of individual sources present in the sample without the option to consider the quality of the individual magnetic recorders (De Groot et al., 2021). To improve upon this method and enable full-vector inversion of micromagnetic microscopy results, Souza-Junior et al. (2024) developed a semi-automated approach based on Euler deconvolution to determine the position and magnetization of dipolar magnetic carriers, purely based on magnetic microscopy imaging. This information is successfully used to invert and quantify the magnetic moments of individual grains in samples. We used this method to estimate the sample-to-sensor distances in our experiments, in addition to the measured sample-to-sensor distances, and evaluated its use and feasibility for MMT.

Here, we present the technicalities and precision of JAMES as well as the results of a series of standoff distance experiments. We discuss the importance of a well-known sample-to-sensor distance for obtaining reliable magnetic moments through the inversion routine of MMT.

2. Methodology

2.1. Sample Description

For this study, we selected a Hawaiian tholeiitic basalt sample from the 1907 Kilauea flow, Hawaii. This sample has previously been used as a case study for micromagnetic measurements (De Groot et al., 2021) and for characterizing individual magnetic moments (Kosters et al., 2023). De Groot et al. (2013) collected this material from site HW03, the rock-magnetic properties of individual iron-oxide grains are described by Ter Maat et al. (2018) and the petrography is described by Kosters et al. (2023). The sample consists of a 3-mm drill core cut from a 30 μm thin section. Iron oxides are distributed throughout the sample, are predominantly cubic in shape, and show only minor weathering related oxidation. Chemical analyses (Ter Maat et al., 2018) indicate that the iron oxides comprise two groups of minerals. The first is ilmenite, a paramagnetic mineral at room temperature (Readman & O'Reilly, 1972). The second is titanomagnetite, which is ferrimagnetic and may hold a remanent magnetization at room temperature (Dunlop & Özdemir, 1997). Prior to magnetic measurements, the sample was polished with a colloid silica suspension to remove surface magnetizations induced by mechanical polishing during sample preparation (De Groot et al., 2021).

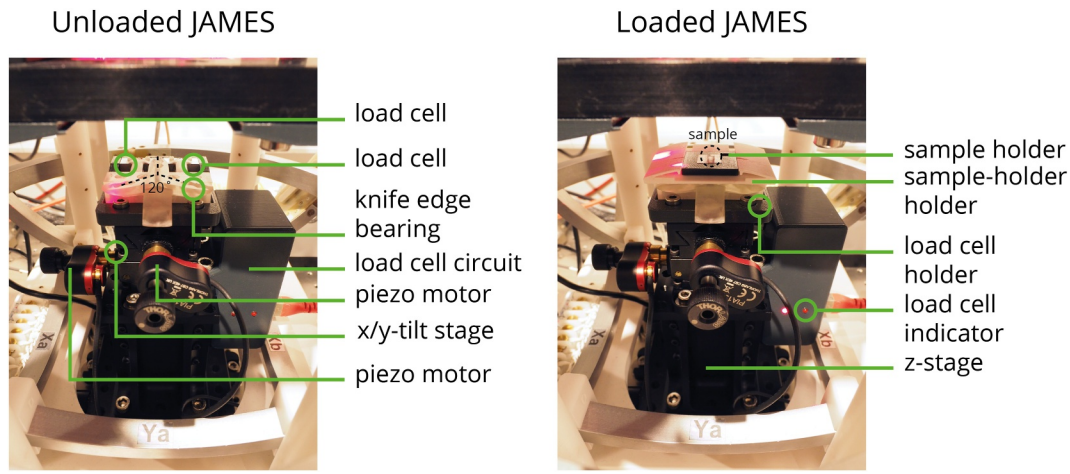


Figure 1. Technical specifications of JAMES. The function of the system's components is explained in the main text. The main objective of JAMES is to achieve precise plan parallel placement of the sample surface against the diamond sensor surface, which is located above the sample.

2.2. Micromagnetic Tomography

Micromagnetic Tomography (De Groot et al., 2018, 2021) combines magnetic surface maps of rock samples with the spatial and dimensional data of the magnetic carriers in the samples, to solve their individual magnetic moments through a least-squares minimization with a unique solution (Fabian & de Groot, 2019). Typically, volcanic samples are used for MMT because they contain numerous small magnetite particles, which are considered ideal recorders of the geomagnetic field that contain a detectable signal.

2.2.1. JAMES

To accurately retrieve reliable magnetic moments using MMT, it is necessary to precisely control the distance between the sample and the diamond sensor of the QDM, as the calculated magnetic moments depend with the third power on this distance (e.g., Cortés-Ortuño et al., 2021). Until now, sample positioning was performed manually. To improve the sample positioning, we developed an automated sample handler for the QDM in our lab, named JAMES (James Automates Manipulation of Earth Samples, Figure 1). JAMES facilitates 1 μm precision sample placement along the x, y, and z axes, and ensures optimal plan-parallel alignment with the diamond sensor through x and y tilt adjustments. The alignment process is controlled by a load cell, which detects sample contact with the diamond while simultaneously preventing excessive pressure that could damage the diamond. JAMES also simplifies repetitive measurements on the same sample area, for instance, after magnetic treatments in different machines.

The core of JAMES comprises a stepper-motor-driven actuator for movement along the x, y, and z directions. Mounted on this three-axis system are x and y axis goniometric tilt platforms, manipulated by piezoelectric motors. Above this, a 3D-printed holder houses two mechanically paralleled load cells monitored by independent circuits for redundancy and sensor safety. The sample holders are placed on top of the load cells and are designed to geometrically lock into place using a system of knife edge bearings. This modular design enables the creation of custom sample holders through 3D printing, allowing the top of the holder to be tailored to accommodate various sample geometries and materials. The sample holders can be adapted to any finely polished flat sample of up to 26 mm in diameter and a thickness ranging from standard thin sections to 15 mm.

The sample-loading process begins with JAMES moving to a designated loading position, approximately 24 mm below the diamond. Once the sample is loaded, JAMES can move upward to a rest position where the top of the sample is approximately 2 mm below the diamond. From this rest position JAMES incrementally moves upward again, now using the load cells to detect contact at a pressure threshold of 15 mN. This value is chosen to ensure sample-sensor contact while maintaining a low enough pressure to prevent any damage to both the sample and sensor. Upon contact, an automated sequence optimizes the x and y tilt adjustments to achieve plan-parallel alignment with the diamond sensor. This alignment can be confirmed by the operator, by looking at the

appearance of the fringe pattern over the entire field of view of the sample. This fully autonomous placement sequence typically takes between 10 and 45 min depending on the geometry, size and surface quality of the sample and JAMES' initial tilt states. The operator can further refine the x and y positions, while maintaining the goniometer angle adjustments. The x and y positions can be saved and reused for successive measurements of the same sample, resulting in a substantial reduction in setup time. This option enables mosaic mapping, where multiple neighboring fields of view can be systematically captured with controlled overlap and combined to create a larger synthetic magnetic map. This capability allows magnetic petrographic analyses over sample areas much larger than a single field of view. The z position can also be adjusted, increasing the distance between the diamond and the sample from the initial direct contact to a maximum of several millimeters while keeping the sample and diamond surfaces plan parallel.

Using a high contrast optical target and given the diffraction limit of the QDM's optical stack (8 μm for 625 nm light), we can evaluate the precision of the sample to diamond distance adjustment. To do this, we increased the test target to diamond distance in seven steps from direct contact to 50 μm and for each step adjusted the position of the optical stack to visually observe the upper and lower positions of the range of maximum image sharpness. When this procedure was carefully executed the observed positions were within 1 μm of the expected positions.

While JAMES substantially enhances sample positioning, it does have some limitations. Achieving the 1 μm alignment accuracy requires a clean sample surface, as dust can prematurely activate the load cell before the sample itself touches the diamond. Additionally, samples must be securely attached to the sample holders, which in turn must lock into place on the knife edge bearings on top of JAMES. Thermal expansion due to the incoming laser light of the QDM can also impact measurements, particularly at larger standoff distances where the sample is not in direct contact with the diamond. In these cases, thermal equilibrium must be reached prior to positioning the sample to minimize changes in the sample-to-sensor distance during QDM measurements.

2.2.2. Quantum Diamond Microscopy

The magnetic surface maps for this study were created with the Quantum Diamond Microscope (QDM) at the paleomagnetic laboratory Fort Hoofddijk of Utrecht University (The Netherlands), which is similar to the set-up described in Glenn et al. (2017). The N15 diamond sensor contains an NV-layer of 1.7 μm thickness. The QDM is housed in a magnetically shielded room with a residual magnetic field of <400 nT to avoid influence of the geomagnetic field during measurements. Prior to the magnetic measurements, the sample was given an isothermal remanent magnetization (IRM) pulse of 140 mT in the direction 180°/00° with a PM4 pulse magnetizer, to provide the sample with a known magnetic direction. This field is expected to exceed the coercivity of most titanomagnetite grains, effectively saturating them. Then, the sample was measured at a series of standoff distances from the sensor in the QDM. The distances were set at 0, 5, 10, 15, 20, 25 and 35 μm with the use of JAMES. The resulting magnetic maps have a maximum field of view of 1,920 × 1,200 pixels with a spatial resolution of 1.20 μm, resulting in 2,304 × 1,440 μm images. During measurements, a bias field of 1.6 mT is applied with a periodically switching polarity. This approach removes any induced magnetization from the remanent magnetization measurements by averaging the images acquired with switched polarities. The QDM measurement settings are listed in Table 1. The results were not binned for data processing and a global fluorescence correction of 0.2 was applied (Fu et al., 2020; Volk et al., 2022). The magnetic map is converted to a map with the vertical component (Bz) of the magnetic flux (Fu et al., 2020; Lima & Weiss, 2016) for further interpretation.

2.2.3. Micro-Computed Tomography

The spatial and dimensional data needed for this study (De Groot et al., 2018, 2021; Fabian & de Groot, 2019) were obtained with the Nanotom-S MicroCT at TU Delft (The Netherlands). The scan resolution is 0.75 μm with a field of view of 1,901 × 2,301 pixels, the measurement settings are listed in Table 2. CT scans generate a three-dimensional image of the sample, and the data interpretation is based on the large attenuation contrast between the high-density magnetic carriers and the surrounding low-density silicate minerals (Cnudde & Boone, 2013). The data is processed with Dragonfly software (ORS), which makes it possible to integrate the QDM data with the nanoCT scans into a single environment. The CT-data are first processed using a median filter to reduce noise, followed by a K-means filter to categorize the data into groups based on density. The group that contains the high-density voxels is processed further, as this group represents the iron oxides in the sample. The attenuation

Table 1
QDM Measurement Settings

Settings	Sample HW03
Exposure time (μs)	13,000
Camera frame time (μs)	13,500
Microwave power (dBm)	−6
Number of sweeps	16
Start frequency 1 (GHz)	2.806
End frequency 1 (GHz)	2.834
Start frequency 2 (GHz)	2.899
End frequency 2 (GHz)	2.927
Frame pairs per frequency	20

threshold is set at the minimum value of this high-density group to ensure that all magnetic grains in the sample are identified. If any non-magnetic grains are unintentionally included, the MMT inversion will assign a (near) zero magnetization to those grains. The adjacent, interconnected voxels in the high-density group are merged into grains with a 26-voxel approach, where voxels that touch, even by one single corner, are grouped into a single magnetic grain. For these grains the size, shape, and location are now known. All grains with <10 voxels are removed from the data set, as they are deemed too small for reliable imaging due to noise interference.

2.2.4. Data Set Co-Registration

The QDM is an optical instrument and it is capable of capturing images of the sample surface under LED illumination. To link the data sets, grains identified in the CT scans are mapped to corresponding surface grains visible in the LED image obtained by the QDM, see Figure 2 of De Boer et al. (2025) for an illustration of the mapping process. The LED image shares the same coordinate system as the magnetic map obtained by the QDM, therefore the magnetic map and the CT data are automatically aligned within the same coordinate system as well. The grain characteristics can then be exported for further use. The size, shape and position of the grains are used to determine properties such as grain diameter, grain volume, and distance from sample surface. The smallest grains considered in this study have a minimum diameter of 1.5 μm. Since obtaining primary magnetic information is not the objective of the current study, it is not a problem that the smaller, more magnetically stable single vortex to single domain grains of the sample are not included.

2.2.5. Magnetic Moment Calculations

The co-registered magnetic data and CT scans are inverted using the inversion routine as in Cortés-Ortuño et al. (2021). This method uses least squares minimization to calculate the individual magnetic moments in three orthogonal directions per magnetic carrier. Here, the dipole expansion is used for the calculations, further details and access to the numerical libraries are described in Cortés-Ortuño et al. (2024).

The inverted data is further processed by applying an SSR cut-off of 7.4×10^{-4} to remove mathematically incorrect results (Out et al., 2022) from the bulk. An Mr/Ms cut-off value of 0.5 is applied to remove any physically unrealistic grain solutions from the bulk. The remaining grains are then used to assess the significance of a known sample-to-sensor distance in quantitative magnetic microscopy.

2.3. Individual Grain Depth Analysis

Besides the bulk inversions, described in the previous section, we use the individual magnetic moments of eight selected grains (Table 3) to analyze the importance of a known sample-to-sensor distance. We selected grains that show a clear dipole signal in the magnetic surface maps and are sufficiently isolated from neighboring magnetic grains, to avoid contamination of their magnetic surface expression by signals from nearby grains. Additionally, we used the individual inversion and the combined (dual) inversion of two non-isolated grains, for comparison with the results of the isolated grains. The grain properties are derived from CT analysis and the equivalent diameter is calculated from the grain volume, assuming a spherical particle.

Table 2
MicroCT Measurement Settings

Settings	Sample HW03
Source voltage (kV)	120
Source current (μA)	80
Image pixel size (μm)	0.75
Number of projections	1,440

We retrieved the sample-to sensor distances set with JAMES (±1 μm), and we also used the method of Souza-Junior et al. (2024) to estimate the sample-to-sensor distances using Euler deconvolution. Then we compared the inversion results obtained with MMT and the method of Souza-Junior et al. (2024) and determined the influence and significance of sample-to-sensor distance on MMT results.

The authors used ChatGPT (OpenAI) for text editing and language refinement in the preparation of this manuscript. All intellectual contributions, including the research design, data analysis, and conclusions, are solely those of the authors.

Table 3
Properties of Ten Individual Grains Selected for Further Analysis

Grain number	Grain depth (μm)	Grain volume (μm^3)	Equivalent diameter (μm)
Isolated grains			
3987	14.7	$1.849*10^3$	15.22
4113	14.0	$4.539*10^3$	20.54
4125	8.4	$4.964*10^3$	21.16
4155	16.2	$5.668*10^3$	22.12
4198	9.3	$8.417*10^3$	25.24
4243	23.0	$1.231*10^4$	28.66
4246	14.2	$1.249*10^4$	28.80
4288	15.7	$1.963*10^4$	33.47
Non-isolated grains			
1577	25.5	5.638	2.21
4157	8.2	$5.868*10^3$	22.38

Note. Grain depth is the distance from the grain center to the sample surface, determined by CT analysis. The grain volume is also determined from CT analysis and was used to calculate the equivalent diameter.

3. Results

3.1. Distance Results

Table 4 provides an overview of the sample-to-sensor distance determinations done for this study. The distance input is the distance setting of JAMES that was used per experiment. This input was verified by focusing on a high contrast optical target, to evaluate the precision of the JAMES system. The resulting measured distance has a maximum deviation of 1 μm from the distance input. From the surface magnetometry results of the standoff distance experiments with the sample, distances were estimated using the method of Souza-Junior et al. (2024). These estimates tend to be an overestimate for samples measured close to the sensor (<20 μm) and an underestimate when samples are farther removed from the sensor (>25 μm). The JAMES distance inputs, as well as a perturbation of ±1 μm, and the distance estimates are used for calculations of magnetic moments both of the sum

Table 4
Comparison of the Sample-to-Sensor Distances Used for Inversion Calculations in the Current MMT Study

1 Distance input (μm)	2 measured distance (μm)	Δμm (2-1)	3 Distance estimate (μm)	Δμm (3-1)
0	0	0	8.9	8.9
5	5	0	18.7	13.7
10	10	0	18.8	8.8
15	15	0	21.5	6.5
20	20	0	31.4	11.4
25	–	–	23.7	−1.3
30	29	−1	–	–
35	–	–	25.6	−9.4
40	40	0	–	–
50	50	0	–	–

Note. The distance input (1) is the distance setting of JAMES per experiment. The measured distance (2) is the actual distance, reconstructed by focusing on a high contrast optical target to determine the precision of JAMES. A maximum difference of 1 μm with the input distance was measured. The distance estimates (3) are based on the method of Souza-Junior et al. (2024). For shallower experiments (<20 μm) the sample-to-sensor distance is typically overestimated, while for deeper experiments (>25 μm) the sample-to-sensor distance is underestimated.

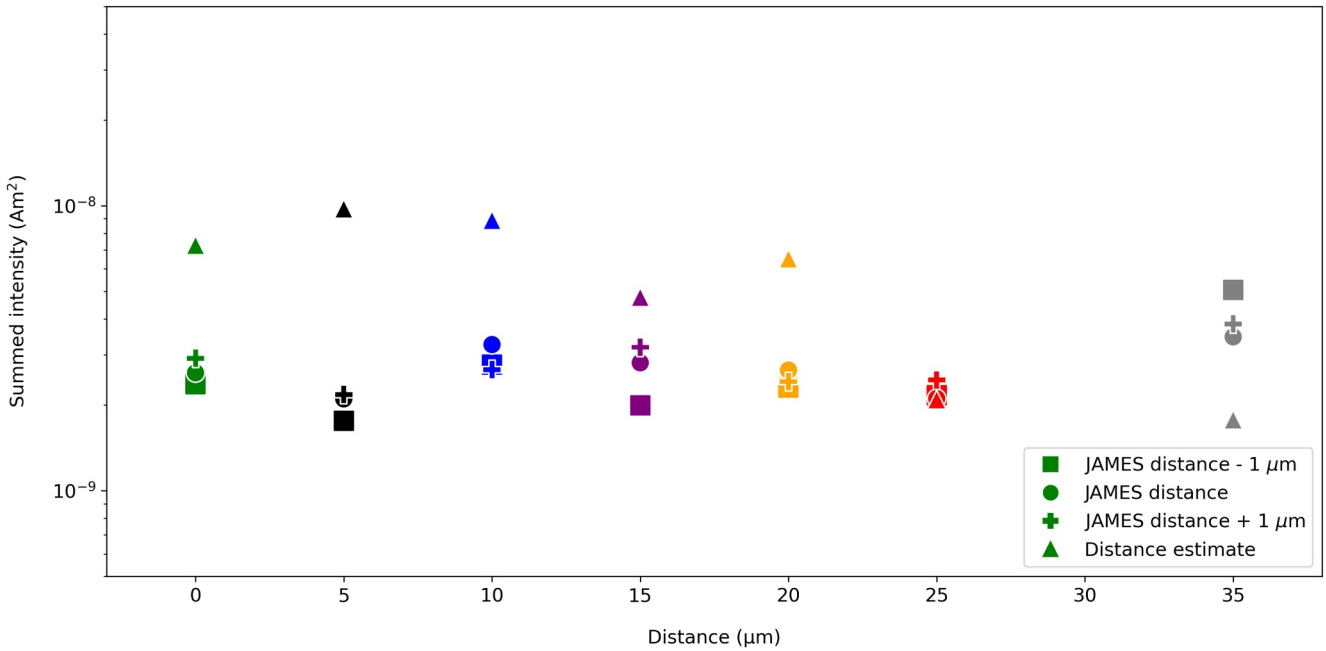


Figure 2. Summed intensity of the grains in the sample against the distance of the sample to the sensor of the QDM. The intensities of the distance experiments are calculated for 4 sample-to-sensor distances: the distance setting of JAMES (JAMES distance), the distance setting of JAMES minus 1 μm (JAMES distance −1 μm), the distance setting of JAMES plus 1 μm (JAMES distance +1 μm), and the estimated distance using the method of Souza-Junior et al. (2024). The summed intensity values of the latter differ up to half an order of magnitude from the intensities calculated with the distance setting.

of all grains and of individual grains, to determine the importance of a known sample-to-sensor distance for quantitative results determined with Micromagnetic Tomography.

3.2. Summed Results

Before the series of standoff distance experiments was carried out, the sample was imparted with an IRM pulse of 140 mT applied parallel to the sample surface in the direction of 180°/00°. It is important to note that the magnetic state of the sample was not changed during the distance experiments, therefore we expect to retrieve an identical summed intensity and summed direction with every measurement distance. We inverted the results and the magnetic moments per grain were summed to determine the summed intensity and the summed direction of the sample per distance experiment. The goal is to determine whether the imparted IRM direction can be retrieved from the data and what the importance of a known sample-to-sensor distance is for these calculations. It is important to note that all results were filtered using the SSR and Mr/Ms cut-offs as described in the methods section.

The summed intensities across the distance experiments (Figure 2) are relatively constant when using the distance setting of JAMES ±1 μm. They differ at most a factor of 2 across the different experiments. When the distance estimates are used, larger summed intensity differences are found across the distance experiments, with a maximum difference of almost an order of magnitude. The values of the summed intensities calculated with the JAMES distance setting and with the distance estimate differ up to half an order of magnitude within the same experiment.

The vector angle deviation is the angle of the summed direction in the sample with the imparted IRM direction parallel to the sample surface in the direction of 180°/00°. Therefore, the maximum possible vector angle deviation is 180°. The results (Figure 3) vary strongly across the distance experiments, and the angle ranges from 14° to 56°. The used distance (JAMES distance input ±1 μm or the distance estimate) does not consistently affect the vector angle deviation. Within the same experiment, the maximum difference between the results of the used distances equals 20°.

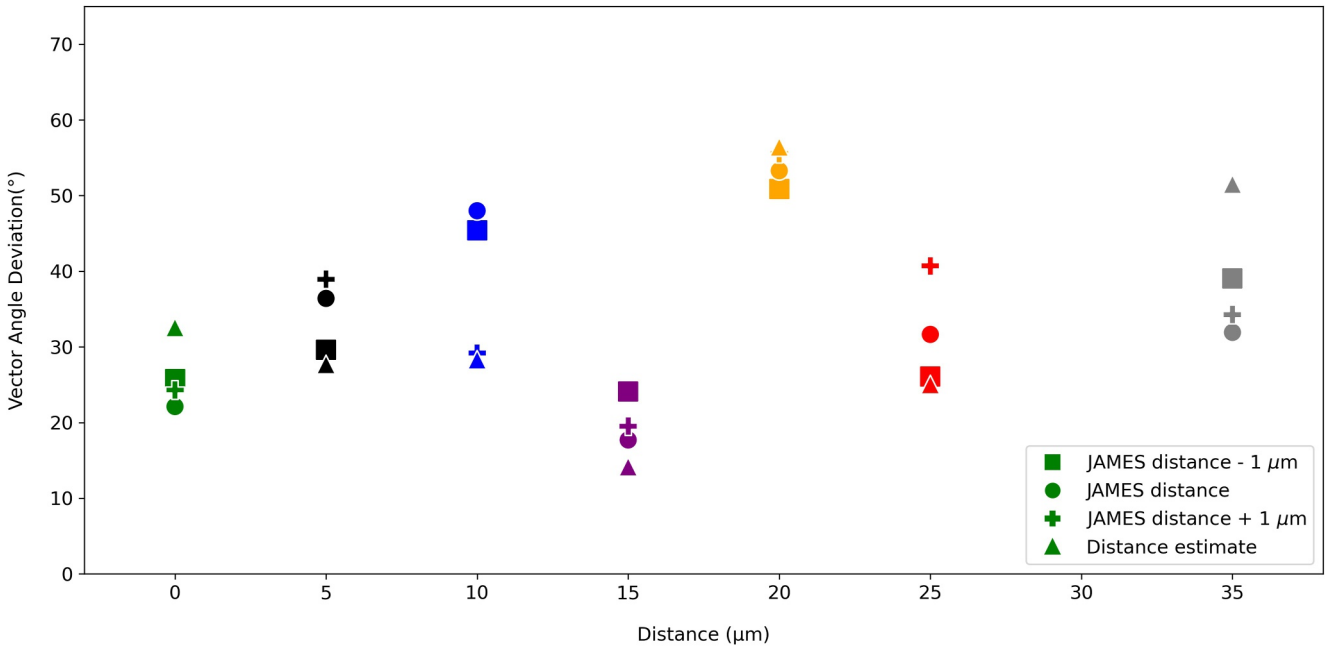


Figure 3. Vector angle deviation of the summed direction of the grains in the sample against the distance of the sample to the sensor of the QDM. The vector angle deviations of the distance experiments are calculated for 4 sample-to-sensor distances: the distance setting of JAMES (JAMES distance), the distance setting of JAMES minus 1 μm (JAMES distance −1 μm), the distance setting of JAMES plus 1 μm (JAMES distance +1 μm), and the estimated distance using the method of Souza-Junior et al. (2024). There is no notable difference between the latter and the directions calculated with the distance setting.

3.3. Individual Grain Results

Besides a bulk inversion, we also inverted individual magnetic grains. The magnetic moments per distance experiment per grain were calculated to determine whether the imparted IRM can be retrieved from the data and to determine the importance of a known sample-to-sensor distance for these calculations. Eight individual grains with an isolated, dipolar signal were selected for this analysis. Furthermore, two grains were selected that are not isolated and optically show one dipole signal on the Bz-map from the QDM (Figure 4). A 30 μm × 30 μm area around each grain was selected to ensure that only (the field of) the grain of interest was included in the inversion of the individual sources. The properties of the grains are listed in Table 3, it should be noted that all are multi-domain (MD) grains, when considering their equivalent diameter.

The calculated magnetic moments per grain are shown against sample-to-sensor distance (Figure 5). For most grains, a consistent magnetic moment is determined across the distance experiments. When the JAMES distance ±1 μm is used, the magnetic moments vary by at most a factor of 3 across the experiments. The ±1 μm maximum deviation from the JAMES distances is considerably more important for shallower experiments than for deeper experiments, because the magnetic moment calculations strongly depend on the sample-to-sensor distance, inducing a proportionally larger deviation when the distance is small. For grain 4125 and grain 4198 the magnetic moments seem to increase with deeper experiments, this likely has to do with the following methodological problem. The magnetic moments per grain were calculated by selecting a 30 μm × 30 μm area around the grain and inverting this area. Grain 4125 and 4198 are close to the sensor (Table 3), so this area is probably too small to capture the entire magnetic surface signal of the grains. As a result, the magnetic moment assigned to the grains by the inversion will be too small. At greater grain-to-sensor distances, the total magnetic surface signal falls within the selected area and the inversion assigns a correct magnetic moment to the grains. For grain 4125 in particular, the orientation of the dipole may further contribute to this effect, as it's direction is more out-of-plane than that of the other selected grains. In addition, a common problem in QDM measurements is the sensor field saturation, which occurs when ODMR peaks shift out of the measured frequency range and lead to poor fits. This is visible as enhanced pixelation in areas showing a high magnetic field. However, we typically filter these pixels and remove them from the inversion. It seems that for the 5 μm distance experiment, JAMES was at a larger distance than the distance input setting, since there is a dip in magnetic moment in all grains during that experiment. This

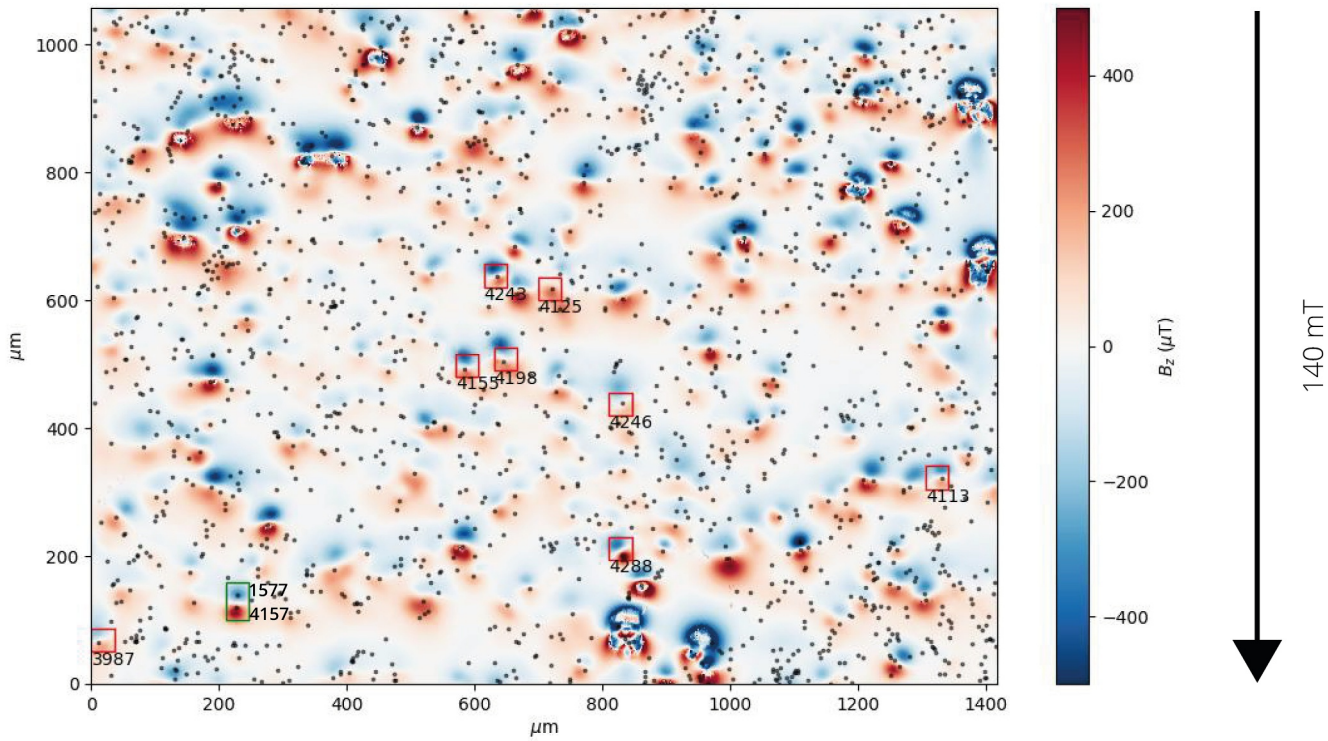


Figure 4. Magnetic flux density map obtained from the QDM with the magnetic centers of the iron oxide grains, as derived from the CT scans, marked as black dots. Positive Bz-values point out of the paper, negative Bz-values point into the paper. The red squares indicate the location of eight isolated grains selected for further analysis. The green rectangle indicates the location of two non-isolated grains selected for further analysis. All grains are labeled by their respective grain number. The sample was given a 140 mT IRM pulse in the direction of the arrow.

discrepancy is likely caused by a setup-related user error. When instead of the JAMES distances the distance estimates are used, the results vary up to an order of magnitude across experiments. The maximum difference in magnetic moments calculated with the JAMES distance setting and the distance estimate is almost an order of magnitude within the same experiment.

The calculated directions per grain are shown per standoff distance experiment (Figure 6). Generally, the grains reproduce the imparted IRM of 180°/00° well, particularly for the experiments shallower than 20 μm. Except for grain 4155, the results become worse for the 20, 25 and 35 μm distance experiments. For grain 3987, 4113, and 4288 the declination changes up to 40° eastwards for the deeper experiments. For grain 4125, 4198, 4243, and 4246 the inclination changes, steepening to 40° for the deeper experiments. This is probably caused by noise interference at larger sample-to-sensor distances. Furthermore, when the sample and sensor are not touching, reflections can occur during measurements, obscuring the obtained images and therefore the derived directions. No substantial difference is observed between the directions determined with the JAMES distances and those using the distance estimates.

In addition to the analysis of the magnetic moments and directions determined from isolated grains with a dipolar magnetic surface expression, we analyzed two non-isolated grains that have a combined dipolar magnetic surface expression (Figure 4). The observations described for the isolated grains (Figure 5) are similar to the observations made for the non-isolated grains (Figure 7). Grain 4157 is larger and shallower than grain 1577 (Table 3). Since this grain is close to the sensor, the inverted area surrounding it is probably not large enough to capture the entire magnetic surface signal of the grain. Therefore, the magnetic moment assigned to the grain is too small at the shallower experiments. When the grain is located further from the sensor, the entire magnetic surface signal falls within the inverted area and a correct magnetic moment is assigned to the grain. The magnetic moments assigned to grain 1577 are more difficult to interpret, likely due to its small size and large distance from the sensor which results in a small surface expression of the magnetic signal. The SSR of this deep grain is below the SSR cut-off.

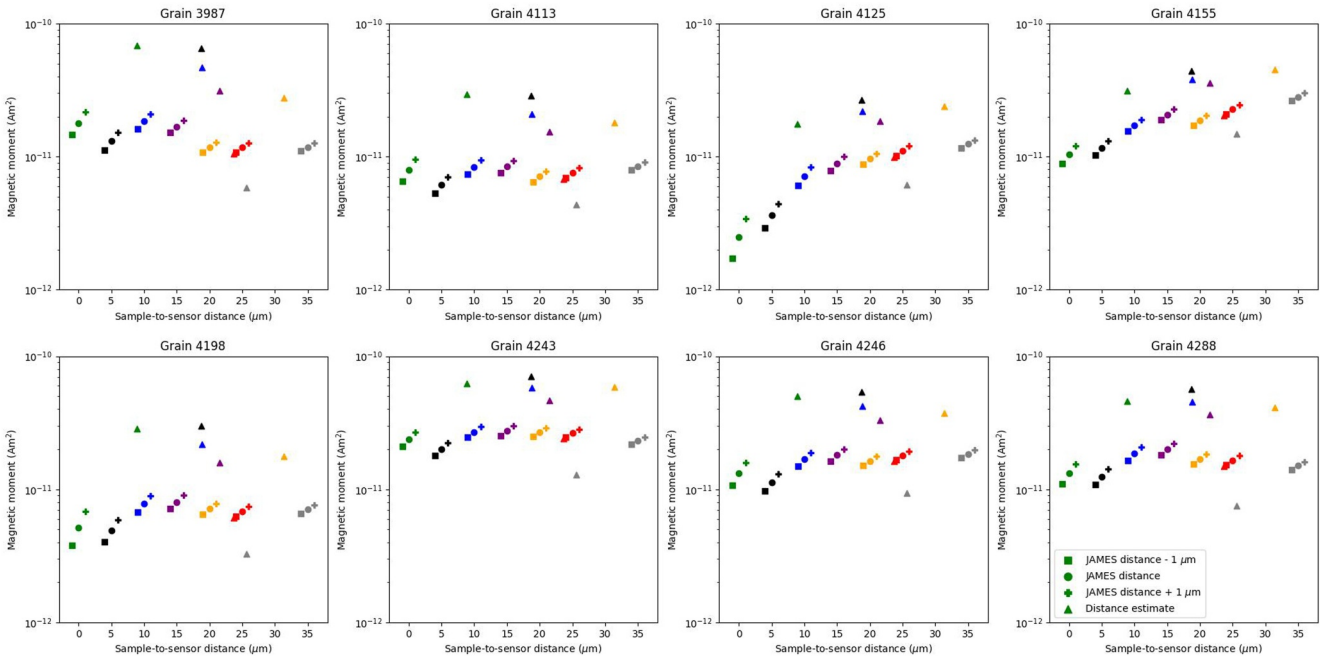


Figure 5. Magnetic moment plotted for 8 individual grains, per distance experiment. For every distance experiment, 4 sample-to-sensor distances were used to calculate the magnetic moments: the distance setting of JAMES (JAMES distance), the distance setting of JAMES minus 1 μm (JAMES distance −1 μm), the distance setting of JAMES plus 1 μm (JAMES distance +1 μm), and the estimated distance using the method of Souza-Junior et al. (2024). The magnetic state of the individual grains does not change across the distance experiments, which is evident in most plots using JAMES distances except for grain 4125 and grain 4198 where the calculated magnetic moments increase with distance. Calculated results using a distance estimate are more erratic.

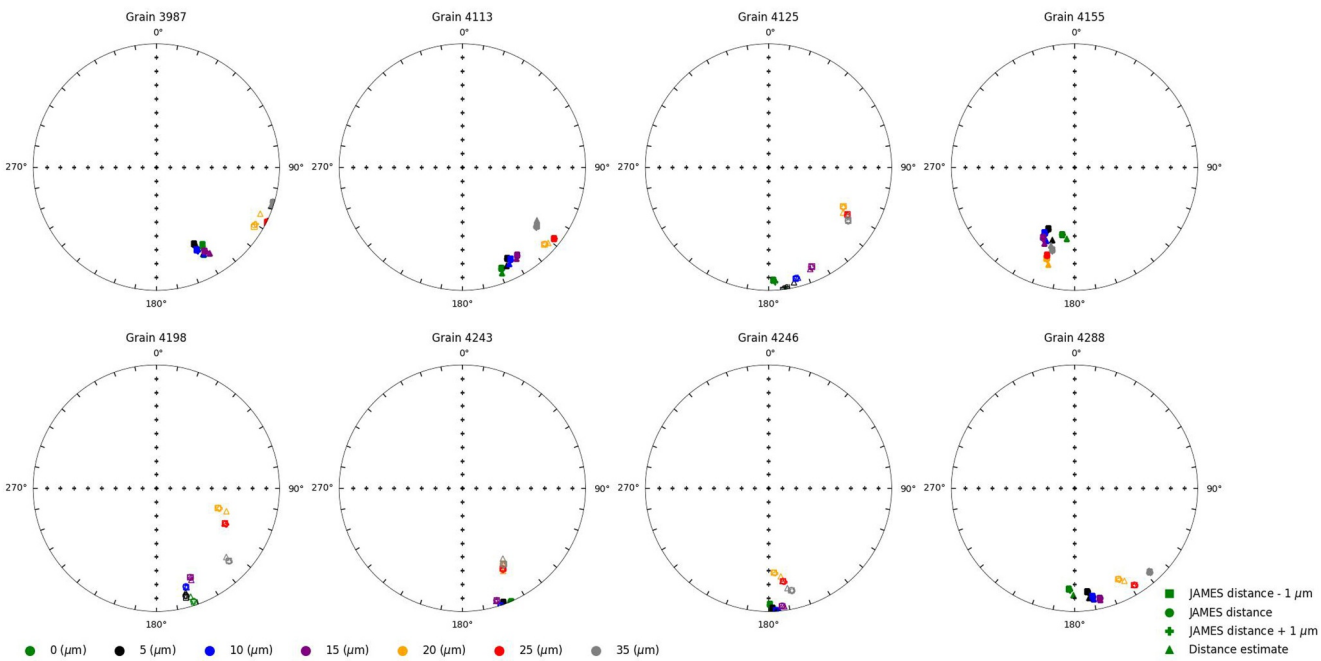


Figure 6. Directions plotted for eight individual grains, per distance experiment. For every distance experiment, four sample-to-sensor distances were used to calculate the directions: the distance setting of JAMES (JAMES distance), the distance setting of JAMES minus 1 μm (JAMES distance −1 μm), the distance setting of JAMES plus 1 μm (JAMES distance +1 μm), and the estimated distance using the method of Souza-Junior et al. (2024). The magnetic state of the grains does not change across the distance experiments, which is somewhat evident in the stereoplots. Most data points plot near the imparted 180°/00° direction, especially for the shallower distance measurements. Calculated results using a distance estimate do not noticeably differ from the results calculated with the JAMES distances.

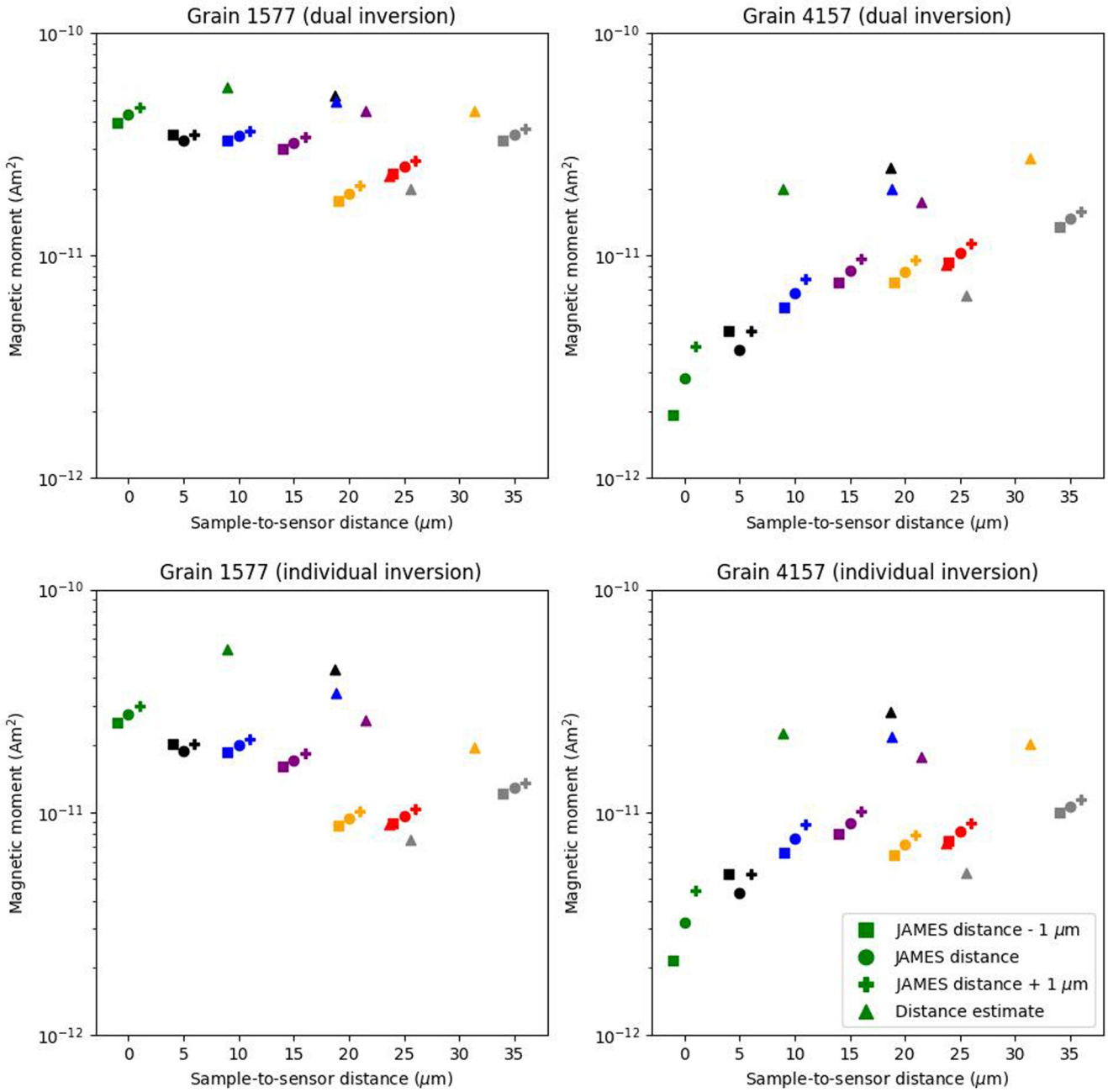


Figure 7. Magnetic moment derived from an individual inversion and a dual inversion of two grains, per distance experiment. For every distance experiment, four sample-to-sensor distances were used to calculate the magnetic moments: the distance setting of JAMES (JAMES distance), the distance setting of JAMES minus 1 μm (JAMES distance −1 μm), the distance setting of JAMES plus 1 μm (JAMES distance +1 μm), and the estimated distance using the method of Souza-Junior et al. (2024). The magnetic state of the grains does not change across the distance experiments.

Therefore, it would be automatically excluded in a standard MMT inversion, in contrast to an individual grain or dual grain inversion.

A difference can be observed in the directions of the isolated grains (Figure 6) and those of the non-isolated grains (Figure 8). The calculated directions of the isolated grains generally reproduce the imparted IRM well, particularly at sample-sensor distances <20 μm. The non-isolated grain 1577 shows a different pattern, when it is inverted individually, the directions are off by up to 90° in declination and 90° in inclination. When the dual inversion is carried out, the directions improve substantially, and the shallow experiments reproduce the IRM

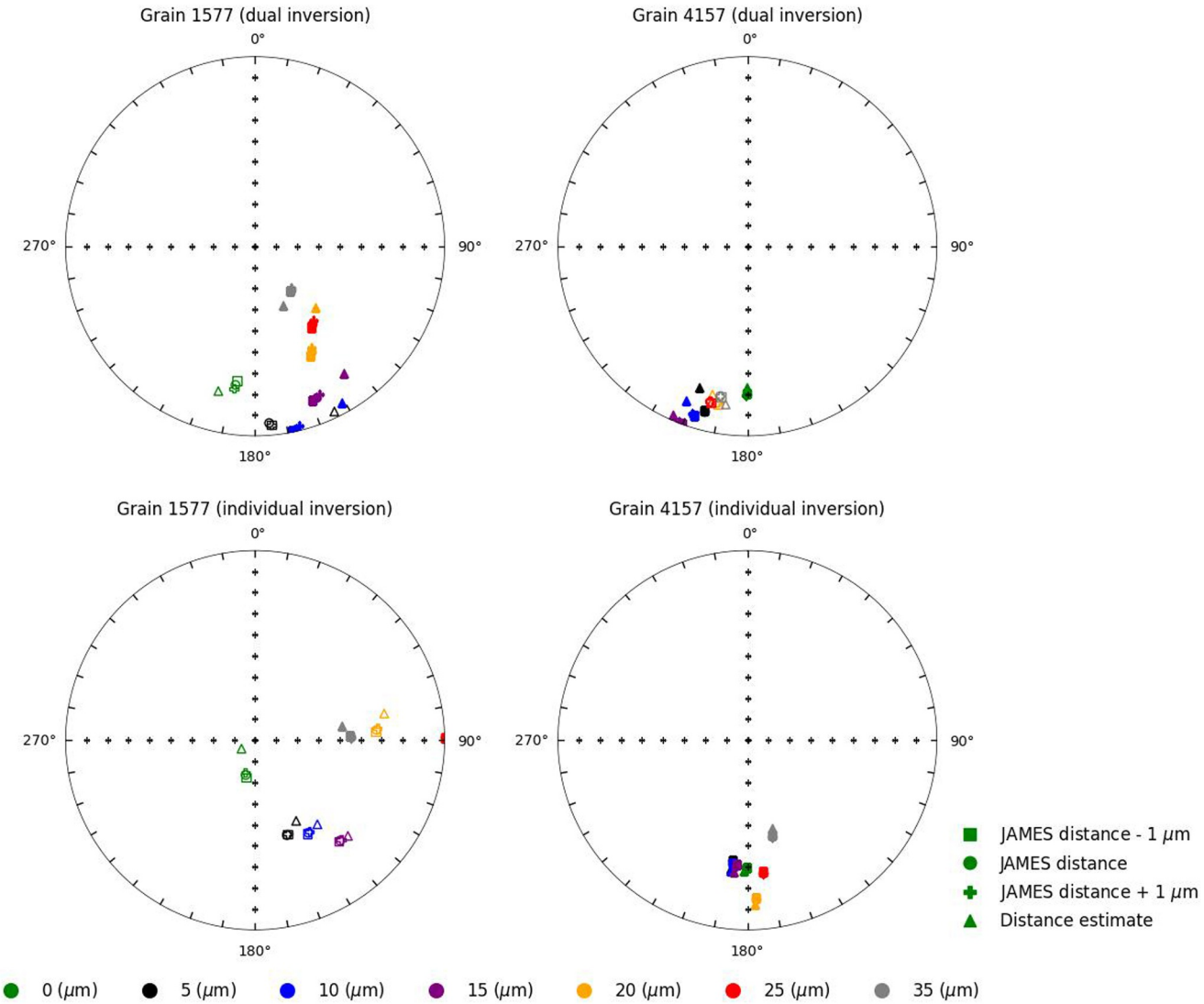


Figure 8. Directions derived from an individual inversion and a dual inversion of two grains, per distance experiment. For every distance experiment, four sample-to-sensor distances were used to calculate the directions: the distance setting of JAMES (JAMES distance), the distance setting of JAMES minus 1 μm (JAMES distance −1 μm), the distance setting of JAMES plus 1 μm (JAMES distance +1 μm), and the estimated distance using the method of Souza-Junior et al. (2024). The magnetic state of the grains does not change across the distance experiments, which is somewhat evident in the stereoplots. Most data of the shallower distance measurements plot near the imparted 180°/00° direction. Calculated results using a distance estimate do not noticeably differ from the results calculated with the JAMES distances.

direction well. This shows the importance of assigning the magnetic surface expression to the correct grain. No substantial difference is observed between the directions determined with the JAMES distances and those using the distance estimates.

4. Discussion

4.1. Performance of JAMES Distances

Summed intensities are compared with summed directions (Figures 2 and 3). Although no quantitative estimate exists for realistic summed intensity values, the summed intensity is calculated from realistic individual magnetic moments with a maximum Mr/Ms ratio of 0.5. Given the imparted IRM of 140 mT, the magnetite grains are expected to have a (near) saturated remanence. The summed intensity values calculated with the JAMES distances are constant across all distance experiments. This indicates that the experiments and the calculations successfully reproduce the summed intensity of a sample across different sample-to-sensor distances. In contrast,

the summed direction results show more complex behavior. The vector angle deviation of the summed direction with the imparted IRM direction ranges from 17° to 53° across distance experiments, without a clear relation to the sample-to-sensor distance. No definitive explanation for this observation was found, although it is consistent with the results reported in other ARM/IRM studies (e.g., De Groot et al., 2021; Fu et al., 2023). Therefore, these are considered to represent reasonably well-defined direction determinations.

Second, the performance of magnetic moments of individual grains is compared with the performance of the directions determined from individual grains (Figures 5 and 6). All individual grains used for this study are >1.5 μm in diameter and are considered to represent MD grains. These grains can optimize their internal domain structure to achieve a local energy minimum. We assume that the optimal domain structure represents the direction of the imparted magnetic field. For most grains, the magnetic moment values calculated with JAMES distances are constant across the distance experiments. This indicates that the experiments and the calculations successfully reproduce the magnetic moments for different sample-to-sensor distances. From the grains that show variation in magnetic moments across the experiments, it became evident that the area selected for inversion around each grain should be carefully considered. If the area is too small, part of the grain's magnetic surface signal is excluded in the inversion, leading to an underestimation of the magnetic moment. Selecting too large of an area introduces noise into the inversion, leading to inaccurate magnetic moments. The directions obtained from individual grain inversions are adequate but tend to deviate 15°–20° eastward from the imparted IRM direction. This may be a methodological issue rather than a problem within the inversion routine. However, this remains unconfirmed, since we could not identify an obvious mistake in the application of the IRM pulse, nor in the sample mounting process. At standoff distances >20 μm, the deviation of the grain directions from the imparted IRM direction becomes larger in terms of inclination and/or declination. Since the magnetic surface flux decays exponentially with distance, the magnetic surface expression of a grain decreases toward noise levels, making it increasingly difficult to determine a precise direction, potentially explaining the observed results. From the individual inversion of non-isolated grains (Figures 7 and 8) it is clear that the quality of the magnetic moment and direction decrease when the magnetic surface signal cannot be assigned to the correct grain. This reconfirms the importance of using spatial and dimensional information of the magnetic carriers in quantitative interpretations. It also highlights the value of applying an SSR cut-off, which excludes individual grains that cannot be reliably solved by the inversion.

Last, both the individual magnetic moments and the summed intensities obtained from all grains (Figures 2 and 5) are constant across the distance experiments using the JAMES distances. However, a difference is observed when comparing the individual grain directions with the summed directions obtained from all grains (Figures 3 and 6). At the individual grain level, experiments with a lower sample-to-sensor distance lead to better results. This trend is not observed in the summed results. To explain this observation, the properties of additional grains need to be studied. The grains that were selected for this study differ in size, shape, and location, but no clear relation with the direction deviations can be distinguished.

4.2. Performance of Distance Estimates

We used the method of Souza-Junior et al. (2024) to assess its feasibility and practical use in MMT. The signals of the magnetic surface scans were used to determine the sample-to-sensor distance, which resulted in an overestimate of the distance in shallower experiments (<20 μm) and an underestimate of the distance in deeper experiments (>25 μm). As a result, the summed intensities and individual magnetic moments using these distance estimates vary by up to an order of magnitude across the distance experiments. Despite this limitation, the imparted IRM direction can be accurately retrieved with the distance estimates, both for the summed directions and the individual grain directions. It should be noted that the latter is valid for grains that are isolated sources with a clear dipolar magnetic surface expression. If either of these conditions is violated, it is impossible to precisely estimate the locations and dimensions of the magnetic grains, these limitations are acknowledged in Souza-Junior et al. (2024). Nonetheless, when the boundary conditions are met, the method of Souza-Junior et al. (2024) proves to be accurate and far less time-consuming than a full MMT workflow. However, information on the position and dimension of the magnetic carriers and a known sample-to-sensor distance are necessary to calculate accurate magnetic moments for individual grains when the carriers are non-isolated or have a non-dipolar magnetic surface expression. This is common for typical MMT samples, which usually consist of volcanic material with a high density of magnetic grains. For such samples, distance estimation is not a reliable basis for inverting the results to magnetic moments. An alternative approach was proposed by Sinimbu et al. (2025), who developed a method for

estimating the magnetic moment from non-dipolar sources, which may be more suitable for some samples, given that they have a low magnetic grain density.

For all inversions in this study, only dipoles were fitted, representing a simplified approximation of the magnetic state of the grains in the samples. Spherical harmonic multipole expansions (Cortés-Ortuño et al., 2021) describe more complex magnetic systems in grains, which is relevant for large grains displaying multidomain behavior and grains close to the scanning surface of the sample. Magnetic maps of isolated grains often differ from that of a magnetic dipole and solving for more complex magnetization patterns increases the interpretation accuracy (Lima et al., 2023). Spherical harmonics become particularly relevant for grains in the single vortex and MD range, which often exhibit non-dipolar characteristics (Nagy et al., 2017), and when measurements are performed at <1 μm sample-to-sensor distance (Cortés-Ortuño et al., 2022).

4.3. Advancing Quantitative Micromagnetic Analysis

We have demonstrated the importance of a known sample-to-sensor distance for quantitative interpretations using Micromagnetic Tomography. A system controlling this distance, such as our in-house developed automated sample placement system JAMES, is therefore an essential component of the experimental procedure. An alternative approach pursued by for example Rietwyk et al. (2024) involves moving the sensor toward the sample instead. Their set-up enables standoff distances below 500 nm, allowing for high-resolution magnetic microscopy. However, their approach does not permit the sample to be positioned at defined distances from the sensor.

The development of JAMES is part of the ongoing improvement of MMT and magnetic microscopy in general. With JAMES routine measurement of accurate magnetic signals at a well-defined sample-to-sensor distance in a Quantum Diamond Microscope is enabled by automated positioning and distance control. This is a substantial advancement in facilitating paleomagnetic and rock-magnetic applications of Micromagnetic Tomography and magnetic microscopy in general.

5. Conclusion

Micromagnetic Tomography is a powerful tool for rock-magnetic and paleomagnetic interpretations of the magnetic signal of individual grains in rock samples. To improve the accuracy of MMT results, we developed an automated sample placement system (JAMES), designed to optimize sample placement during QDM measurements. JAMES can place a polished, flat sample plan parallel against the diamond sensor of the QDM or at a desired distance from the sensor with a vertical precision of ±1 μm, with additional precise control in the x and y direction. This enables simple, consistent, and replicable QDM measurements at a replicable x and y position and a precisely known sample-to-sensor distance.

We evaluated the importance of the sample-to-sensor distance for the accurate retrieval of quantitative magnetic information with MMT. A constant summed intensity can be retrieved for various measurement distances, at least up to 35 μm. A constant magnetic moment can be retrieved from individual MD grains in this distance range as well. We can roughly retrieve an imparted IRM direction across various measurement distances, up to 35 μm, from the summed signal of all grains. An imparted direction can be retrieved from individual MD grains for sample distances up to 20 μm. The differences between individual grain directions and summed directions cannot be explained yet and need further investigation. The summed results are derived from a total of 736 interpretable grains, which equals ca. 16,000 interpretable grains per mm^3.

The performance of the distance estimation method from Souza-Junior et al. (2024), was evaluated for its applicability in MMT. The distance estimates work reasonably well for retrieving summed directions and directions from isolated grains with a dipolar surface expression across different sample-to-sensor distance experiments. However, when retrieving summed intensities or individual magnetic moments across different sample-to-sensor distances, the distance estimates introduce significant limitations. For typical MMT samples, with a high-density population of magnetic grains, precise determination of grain positions is needed. Therefore, for reliable magnetic moment calculations and robust quantitative paleomagnetic interpretations for MMT, both information from CT-imaging as well as a controlled sample-to-sensor distance during measurements are essential.

JAMES is now an integral part of the standard procedure for acquiring QDM data in MMT. By ensuring a precisely known sample-to-sensor distance, JAMES enables reliable and accurate magnetic moment determinations. These findings open new possibilities for high-resolution, quantitative paleomagnetic studies.

Conflict of Interest

The authors declare no conflicts of interest relevant to this study.

Availability Statement

The data used in this study has been uploaded to Yoda and can be found under https://doi.org/10.24416/UU01-6DYWS0.

Acknowledgments
This project has received funding from the European Research Council (ERC) under the European Union's Horizon 2020 research and innovation program (Grant 851460 to LVdG).

References

Blakely, R. J. (1996). *Potential theory in gravity and magnetic applications*. Cambridge University Press. https://doi.org/10.1017/CBO9780511549816

Brenner, A. R., Fu, R. R., Kylander-Clark, A. R. C., Hudak, G. J., & Foley, B. J. (2022). Plate motion and a dipolar geomagnetic field at 3.25 Ga. *Proceedings of the National Academy of Sciences*, *119*(44), e2210258119. https://doi.org/10.1073/pnas.2210258119

Cnudde, V., & Boone, M. N. (2013). High-resolution X-ray computed tomography in geosciences: A review of the current technology and applications. *Earth-Science Reviews*, *123*, 1–17. https://doi.org/10.1016/j.earscirev.2013.04.003

Cortés-Ortuño, D. I., Fabian, K., & de Groot, L. V. (2021). Single particle multipole expansions from micromagnetic tomography. *Geochemistry, Geophysics, Geosystems*, *22*(4), 7031. https://doi.org/10.1029/2021GC009663

Cortés-Ortuño, D. I., Fabian, K., & de Groot, L. V. (2022). Mapping magnetic signals of individual magnetite grains to their internal magnetic configurations using micromagnetic models. *Journal of Geophysical Research: Solid Earth*, *127*(5), e2022JB024234. https://doi.org/10.1029/2022JB024234

Cortés-Ortuño, D. I., Out, F., Kosters, M. E., Fabian, K., & de Groot, L. V. (2024). Micromagnetic tomography: Numerical libraries. *Computers & Geosciences*, *185*, 105555. https://doi.org/10.1016/j.cageo.2024.105555

De Boer, R. A., Wielens, D. H., & de Groot, L. V. (2025). Improving co-registration of geoscientific imaging datasets with micro-sized marker structures on rock samples. *Geoscientific Instrumentation, Methods and Data Systems*, *14*(2), 325–334. https://doi.org/10.5194/gi-14-325-2025

De Groot, L. V., Biggin, A. J., Dekkers, M. J., Langereis, C. G., & Herrero-Bervera, E. (2013). Rapid regional perturbations to the recent global geomagnetic decay revealed by a new Hawaiian record. *Nature Communications*, *4*(1), 2727. https://doi.org/10.1038/ncomms3727

De Groot, L. V., Fabian, K., Béguin, A., Kosters, M. E., Cortés-Ortuño, D. I., Fu, R. R., et al. (2021). Micromagnetic tomography for paleomagnetism and rock-magnetism. *Journal of Geophysical Research: Solid Earth*, *126*(10), e2021JB022364. https://doi.org/10.1029/2021JB022364

De Groot, L. V., Fabian, K., Béguin, A., Reith, P., Barnhoorn, A., & Hilgenkamp, H. (2018). Determining individual particle magnetizations in assemblages of micrograins. *Geophysical Research Letters*, *45*(7), 2995–3000. https://doi.org/10.1002/2017GL076634

Dunlop, D. J., & Özdemir, Ö. (1997). *Rock magnetism: Fundamentals and frontiers (No. 3)*. Cambridge University Press. https://doi.org/10.1017/CBO9780511612794

Fabian, K., & de Groot, L. V. (2019). A uniqueness theorem for tomography-assisted potential-field inversion. *Geophysical Journal International*, *216*(2), 760–766. https://doi.org/10.1093/gji/ggy455

Fu, R. R., Drabon, N., Wiedenbeck, M., Brenner, A. R., Lowe, D. R., & Borlina, C. S. (2021). Paleomagnetism of 3.5-4.0 Ga zircons from the Barberton greenstone belt, South Africa. *Earth and Planetary Science Letters*, *567*, 116999. https://doi.org/10.1016/j.epsl.2021.116999

Fu, R. R., Lima, E. A., Volk, M. W. R., & Trubko, R. (2020). High-sensitivity moment magnetometry with the quantum diamond microscope. *Geochemistry, Geophysics, Geosystems*, *21*(8), e2020GC009147. https://doi.org/10.1029/2020GC009147

Fu, R. R., Maher, B. A., Nie, J., Gao, P., Berndt, T., Folsom, E., & Cavanaugh, T. (2023). Pinpointing the mechanism of magnetic enhancement in modern soils using high-resolution magnetic field imaging. *Geochemistry, Geophysics, Geosystems*, *24*(3), e2022GC010812. https://doi.org/10.1029/2022GC010812

Fu, R. R., Weiss, B. P., Lima, E. A., Harrison, R. J., Bai, X., Desch, S. J., et al. (2014). Solar nebula magnetic fields recorded in the Semarkona meteorite. *Science*, *346*(6213), 1089–1092. https://doi.org/10.1126/science.1258022

Glenn, D. R., Fu, R. R., Kehayias, P., Le Sage, D., Lima, E. A., Weiss, B. P., & Walsworth, R. L. (2017). Micrometer-scale magnetic imaging of geological samples using a quantum diamond microscope. *Geochemistry, Geophysics, Geosystems*, *18*(8), 3254–3267. https://doi.org/10.1002/2017GC006946

Grappone, J. M., van der Boon, A., Fu, R. R., & Biggin, A. J. (2025). Evidence for an exceptionally weak Cambrian geomagnetic field: New paleointensity estimates from the Florida Mountains, New Mexico. *Geochemistry, Geophysics, Geosystems*, *26*(7), e2025GC012234. https://doi.org/10.1029/2025GC012234

Hess, K., Fu, R. R., Piascik, S., Stríkis, N. M., Trindade, R. I. F., Kukla, T., et al. (2024). Investigating speleothem magnetism as a proxy for dust mobilization and rainfall. *Quaternary Science Reviews*, *330*, 108598. https://doi.org/10.1016/j.quascirev.2024.108598

Kellogg, O. D. (1929). *Foundations of potential theory*. Springer Berlin Heidelberg. https://doi.org/10.1007/978-3-642-90850-7

Kosters, M. E., de Boer, R. A., Out, F., Cortés-Ortuño, D. I., & de Groot, L. V. (2023). Unraveling the magnetic signal of individual grains in a Hawaiian lava using micromagnetic tomography. *Geochemistry, Geophysics, Geosystems*, *24*(4), e2022GC010462. https://doi.org/10.1029/2022GC010462

Levine, E. V., Turner, M. J., Kehayias, P., Hart, C. A., Langellier, N., Trubko, R., et al. (2019). Principles and techniques of the quantum diamond microscope. *Nanophotonics*, *8*(11), 1945–1973. https://doi.org/10.1515/nanoph-2019-0209

Lima, E. A., Bruno, A. C., Carvalho, H. R., & Weiss, B. P. (2014). Scanning magnetic tunnel junction microscope for high-resolution imaging of remanent magnetization fields. *Measurement Science and Technology*, *25*(10), 105401. https://doi.org/10.1088/0957-0233/25/10/105401

Lima, E. A., & Weiss, B. P. (2009). Obtaining vector magnetic field maps from single-component measurements of geological samples. *Journal of Geophysical Research*, *114*(B6). https://doi.org/10.1029/2008JB006006

Lima, E. A., & Weiss, B. P. (2016). Ultra-high sensitivity moment magnetometry of geological samples using magnetic microscopy. *Geochemistry, Geophysics, Geosystems*, *17*(9), 3754–3774. https://doi.org/10.1002/2016GC006487

Lima, E. A., Weiss, B. P., Borlina, C. S., Baratchart, L., & Hardin, D. P. (2023). Estimating the net magnetic moment of geological samples from planar field maps using multipoles. *Geochemistry, Geophysics, Geosystems*, *24*(7), e2022GC010724. https://doi.org/10.1029/2022GC010724

Nagy, L., Williams, W., Muxworthy, A. R., Fabian, K., Almeida, T. P., Conbhuí, P. Ó., & Shcherbakov, V. P. (2017). Stability of equidimensional pseudo–single-domain magnetite over billion-year timescales. *Proceedings of the National Academy of Sciences*, *114*(39), 10356–10360. https://doi.org/10.1073/pnas.1708344114

Oda, H., Kumagai, S., Fujiwara, K., Matsuzaki, H., Wagatsuma, H., Oogane, M., et al. (2024). Advancement in scanning magnetic microscopy utilizing high-sensitivity room-temperature tmr sensors for geological applications. *Earth Planets and Space*, *76*(1), 1–13. https://doi.org/10.1186/s40623-024-02118-0

Out, F., Cortés-Ortuño, D. I., Fabian, K., van Leeuwen, T., & de Groot, L. V. (2022). A first-order statistical exploration of the mathematical limits of micromagnetic tomography. *Geochemistry, Geophysics, Geosystems*, *23*(4), e2021GC010184. https://doi.org/10.1029/2021GC010184

Qi, L., Muxworthy, A. R., Baker, E. B., Cao, X., Allerton, S., Bryson, J. F. J., & Zhang, Y. (2025). Quantifying serpentinization-driven remagnetization from ridge axis to subduction zone using quantum diamond microscopy. *Journal of Geophysical Research: Solid Earth*, *130*(10), e2025JB031606. https://doi.org/10.1029/2025JB031606

Readman, P. W., & O'Reilly, W. (1972). Magnetic properties of oxidized (cation-deficient) titanomagnetites (Fe, Ti, $X)_3O_4$. *Journal of Geomagnetism and Geoelectricity*, *24*(1), 69–90. https://doi.org/10.5636/jgg.24.69

Rietwyk, K. J., Shaji, A., Robertson, I. O., Healey, A. J., Singh, P., Scholten, S. C., et al. (2024). Practical limits to spatial resolution of magnetic imaging with a quantum diamond microscope. *AVS Quantum Science*, *6*(4), 044402. https://doi.org/10.1116/5.0230098

Scholten, S. C., Healey, A. J., Robertson, I. O., Abrahams, G. J., Broadway, D. A., & Tetienne, J. P. (2021). Widefield quantum microscopy with nitrogen-vacancy centers in diamond: Strengths, limitations, and prospects. *Journal of Applied Physics*, *130*(15), 150902. https://doi.org/10.1063/5.0066733

Sinimbu, L. A., Reis, A., Marques Ereias, B., Noris, L. F., Yokoyama, E., Mendoza, A. F., et al. (2025). Estimating the geometry of magnetization distributions within a geological sample from magnetic microscopy images. https://doi.org/10.2139/ssrn.5098740

Souza-Junior, G. F., Uieda, L., Trindade, R. I. F., Carmo, J., & Fu, R. R. (2024). Full vector inversion of magnetic microscopy images using Euler deconvolution as prior information. *Geochemistry, Geophysics, Geosystems*, *25*(7), e2023GC011082. https://doi.org/10.1029/2023GC011082

Steele, S. C., Fu, R. R., Volk, M. W. R., North, T. L., Brenner, A. R., Muxworthy, A. R., et al. (2023). Paleomagnetic evidence for a long-lived, potentially reversing martian dynamo at ~3.9 Ga. *Science Advances*, *9*(21), eade9071. https://doi.org/10.1126/sciadv.ade9071

Ter Maat, G. W., Pennock, G. M., & de Groot, L. V. (2018). A chemical, crystallographic and magnetic characterisation of individual iron-oxide grains in Hawaiian lavas. *Scientific Data*, *5*(1), 1–9. https://doi.org/10.1038/sdata.2018.162

Volk, M. W. R., Fu, R. R., Trubko, R., Kehayias, P., Glenn, D. R., & Lima, E. A. (2022). Qdmlab: A matlab toolbox for analyzing quantum diamond microscope (qdm) magnetic field maps. *Computers & Geosciences*, *167*, 105198. https://doi.org/10.1016/j.cageo.2022.105198